Supplementary Information

Benzene Adsorption: A Significant Inhibitor for the Hydrogen Oxidation Reaction in Alkaline Conditions

Ivana Matanovic,[‡[a,b]] *Hoon Taek Chung*[‡[c]] *and Yu Seung Kim*[*[c]]

[a] Department of Chemical and Biological Engineering, University of New Mexico, Albuquerque, New Mexico 87231 USA

[b] T-1: Physics and Chemistry of Materials, Los Alamos National Laboratory, Los Alamos, New Mexico 87545 USA

[c] MPA-11: Materials Synthesis and Integrated Devices, Los Alamos National Laboratory, Los Alamos, New Mexico 87545 USA

*yskim@lanl.gov

Methods

Materials. 0.1 M aqueous solutions of organic cations were prepared from TMAOH (25% in water, ACROS) and BTMAOH (40% in water, Sigma-Aldrich). 0.1 M NaOH solutions were made with NaOH pellets (99.99%, Alfa Aesar). 20 wt_{metal}% Pt/C, Pt_3Mo_1/C, Pt_1Ni_1/C and Pt_1Ru_1/C were obtained from E-TEK. We used Pt_3Mo_1 alloy catalyst instead of Pt_1Mo_1 because the composition of Pt3 to Mo1 is known as most active for hydrogen oxidation.[1] The X-ray diffraction data indicates the bimetallic catalysts form an alloy structure (**Figure S3)**. The catalyst inks were prepared by ultrasonically blending of 10 mg of the Pt or Pt alloy catalysts with 40 μl of 5 wt% Nafion® suspension in alcohol (Solution Technology, Inc.) for 1 hour in 10 ml of de-ionized water (18.2 MΩ cm, Millipore) in an ice bath. Before RDE experiments, 20 μl of the solution was deposited onto the 5.0 mm in diameter glassy carbon electrode, disk geometric area is 0.196 cm^2, which was polished with 0.05 μm alumina, resulting in a catalyst loading of 20 μg_{metal} cm^{-2}.

RDE measurement. RDE measurements were performed using a CHI Electrochemical Station (Model 760D) in a standard three-electrode cell at a room temperature, 25 ± 1 °C. A platinized Pt wire served as a counter electrode and a Hg/HgO (Radiometer Analytical Inc.) in 1.0 M KOH as a reference electrode for alkaline electrolytes and a Ag/AgCl (Bioanalytical Systems Inc.) in 3.0 M NaCl as a reference electrode for acidic electrolyte. All potentials initially measured vs. the Hg/HgO electrode (or Ag/AgCl electrode) were converted to a RHE scale by measuring HOR/HER currents on the Pt/C and the bimetallic catalysts in the same electrolyte, whereby the potential at zero current corresponds to 0.0 V vs. RHE. After the electrolytes were saturated with pure hydrogen, polarization plots were recorded between ca. – 0.1 and 1.2 V vs. RHE at a sweep rate of 5 mV s^{-1} and rotation rate of 900 rpm. After the electrolytes were saturated with nitrogen, the cyclic voltammogram at 25 °C was recorded between 0.0 and 1.2 V vs. RHE at a scan rate of

20 mV s^{-1} at 0 rpm. The RDE measurements were repeated 2-3 times independently to ensure the data reproducibility. Typical standard deviation is 5-10 % of the measured HOR current. The AC impedance was measured from 100 to 0.001 kHz with a voltage perturbation of 5 mV in the hydrogen saturated electrolytes at 0.1 V vs. RHE. We measured the impedance of the RDE in the organic cation solutions. **Figure S4** shows the impedance of Pt/C in 0.1 M TMAOH, BTMAOH, and NaOH. It was noted that the extrapolated high frequency resistance corresponding to the electrolyte resistance were similar, ca. electrolyte resistance were similar, ca. 9.1, 7.5 and 8.2 Ω, for TMAOH, BTMAOH and NaOH, indicating that there is no significant pH effect on our experiments.

The HOR/HER charge transfer coefficient (α) and exchange current density (i_0) for the catalysts were obtained by fitting the HOR/HER kinetic current densities to the Butler-Volmer equation. The exchange current density was normalized by geometric area of the electrode.

Computational details. The electronic structure calculations were performed using generalized gradient approximation (GGA) to density functional theory (DFT) with Perdew-Wang (PW91) exchange-correlation functional[2,3] and projector augmented-wave pseudopotentials[4,5] as implemented in Vienna Ab initio Software Package (VASP)[6-9]. Extended Pt(111), Pt_3Mo_1(111), Pt_1Ni_1(111), and Pt_1Ru_1(111) surfaces were modeled using super cells with the dimensions of 16.80 × 16.80 Å, 16.91 × 16.91 Å, 15.89 × 15.89 Å and 16.48 × 16.48 Å, respectively. These correspond to the unit cells of the size $(3a\sqrt{2} \times 3b\sqrt{2})R\gamma$ where a b, and γ are the cell parameters determined from the bulk calculations. In all the cases we modeled the system using three layers of metal atoms and a vacuum region of 20 Å. To simulate the effect of the bulk, the two top layers and the adsorbed species were allowed to relax until the convergence in energy was 1×10^{-5} eV while the bottom layers were held fixed. The electronic energies were calculated using 4×4×1 k-

point Monkhorts-Pack[10] mesh and Methfessel-Paxton smearing[11] of order 2 with a value of σ = 0.2 to aid convergence. In all the cases, plane-wave basis cutoff was set to 400 eV. The change in the free energy during the adsorption was calculated as

$$\Delta rG = \Delta E_{\mathrm{BTMA}} + \Delta ZPE + T\Delta S$$

where ΔE_{BTMA}, ΔZPE, and ΔS are the change in the electronic energy, zero point energy, and entropy in the adsorption process. Adsorption energy was calculated using the following formula:

$$\Delta E_{\mathrm{BTMA}} = E_{\mathrm{surface+BTMA}} - \left[E_{\mathrm{surface}} + E_{\mathrm{BTMA}}\right]$$

where $E_{surface+BTMA}$ is the energy of BTMA adsorbed on the Pt(111) or alloy surfaces, $E_{surafce}$ is the energy of the clean surface, and E_{ad} is the energy of BTMA in the gas phase. Zero point energies were calculated using the vibrational frequencies obtained from the normal mode analysis. Entropy of BTMA at T = 298 K was calculated using B3LYP/6-31+G(d,p) level of theory and polarizable continuum model as implemented in Gaussian 09 quantum chemical package[12]. The calculations were carried out with the assumption that the change in the solvation of the large organic cations will not have a significant effect on the calculated free energies of adsorption. For the calculations of the local electric field effects on the adsorption energies of BTMA the binding energy was calculated as a function of applied electric field using

$$\Delta E_{\mathrm{BTMA,field}} = E_{\mathrm{surface+BTMA,\,field}} - \left[E_{\mathrm{surface,field}} + E_{\mathrm{BTMA}}\right]$$

where the same field is applied to the surface with and without adsorbed BTMA, but the isolated BTMA cation is in vacuum without a field.

Charge transfer between the metal surfaces and BTMA in the orientation with the highest binding energy is obtained by analyzing the electronic charges calculated using Bader's analysis of charge densities.[13-16]

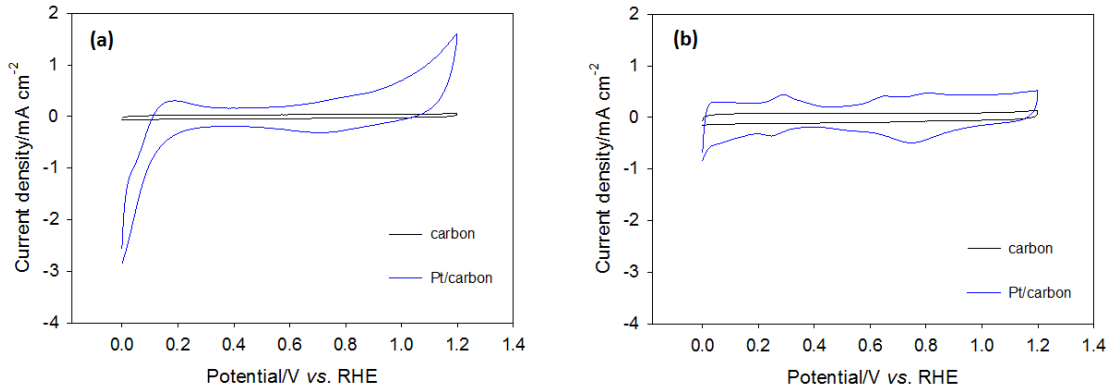

Figure S1. CV of carbon and Pt/C in 0.1 M (a) BTMAOH and (b) TMAOH solutions: the CVs were performed at 25 °C at a scan rate of 20 mV s^{-1} at 0 rpm.

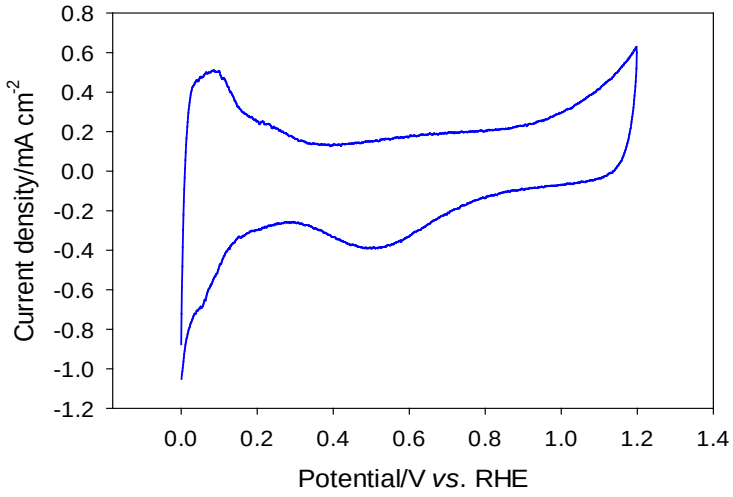

Figure S2. CV of carbon-supported Pt_1Ru_1/C in 0.1 M NaOH; the CVs were performed at 25 °C at a scan rate of 20 mV s^{-1} at 0 rpm.

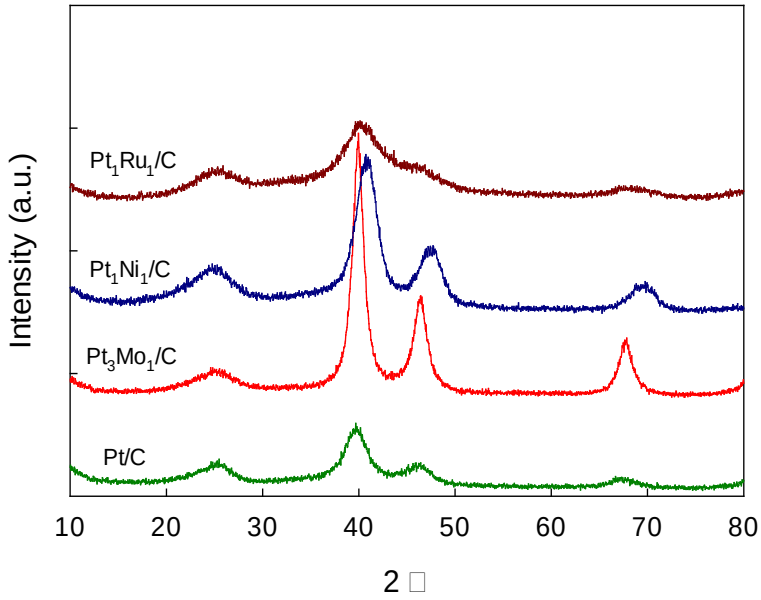

Figure S3. XRD patterns of Pt/C, Pt_3Mo_1/C, Pt_1Ni_1/C, and Pt_1Ru_1/C. These XRD patterns show that all bimetallic catalysts are single phase alloys.

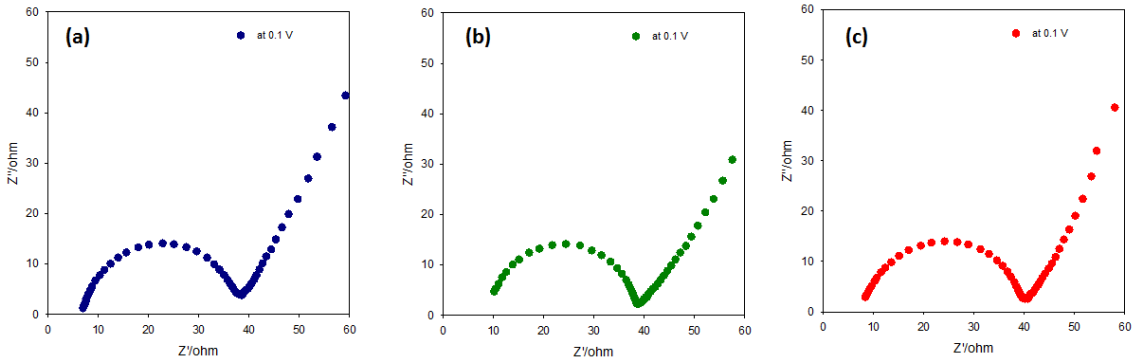

Figure S4. Impedance measured at 900 rpm at 0.1 V vs RHE with Pt/C catalyst in (a) BTMAOH, (b) TMAOH, and (c) NaOH.

Table S1. Adsorption energies for BTMA cation (ΔE_{BTMA}) in eV calculated using DFT with PW91 functional on Pt(111), Pt_3Mo_1(111), Pt_1Ni_1(111), and Pt_1Ru_1(111) surfaces.

orientation/ system	(1)	(2)	(3)	(4)
Pt	-2.30	-2.15	-1.52	-2.15
Pt_3Mo_1	-1.61	-1.67	-0.99	-1.71
Pt_1Ni_1	-1.45	-1.56	-0.47	-1.52
Pt_1Ru_1	-1.32	-1.42	-0.37	-1.39

REFERENCES

1 Jaksic, J. M. Vracar, L. J.; Neophytides, S. G.; Zafeiratos, S.; Papakonstantinou, G.; Krstajic, N. V.; Jaksic, M. M. Sturectural Effects on Kinetic Properties for Hydrogen Electrode Reactions and CO Tolearnace along Mo-Pt Phase Diagram. *Surf. Sci.* **2005**, 598, 156–173.

2 Perdew, J. P.; Chevary, J. A.; Vosko, S. H.; Jackson, K. A.; Pederson, M. R.; Singh, D. J.; Fiolhais, C. Atoms, Molecules, Aolids, and Aurfaces - Applications of the Generalized Gradient Approximation for Exchange and Correlation. *Phys. Rev. B* **1992**, *46*, 6671–6687.

3 Perdew, J. P.; Chevary, J. A.; Vosko, S. H.; Jackson, K. A.; Pederson, M. R.; Singh, D. J.; Fiolhais, C. Atoms, Molecules, Solids, and Surfaces - Applications of the Generalized Gradient Approximation for Exchange and Correlation (Vol 46, Pg 6671, 1992). *Phys. Rev. B* **1993**, *48*, 4978–4978.

4 Blochl, P. E. Projector Augmented-Wave Method. *Phys. Rev. B* **1994**, *50*, 17953-17979.

5 Kresse, G.; Joubert, D. From Ultrasoft Pseudopotentials to the Projector Augmented-Wave Method. *Phys. Rev. B* **1999**, *59*, 1758–1775.

6 Kresse, G.; Hafner, J. Ab-initio Molecular-Dynamics for Liquid-Metals. *Phys. Rev. B* **1993**, *47*, 558–561.

7 Kresse, G.; Hafner, J. Ab-initio Molecular-Dynamics Simulation of the Liquid-Metal Amorphous-Semiconductor Transition in Germanium. *Phys. Rev. B* **1994**, *49*, 14251–14269.

8 Kresse, G.; Furthmuller, J. Efficiency of Ab-initio Total Energy Calculations for Metals and Semiconductors Using a Plane-wave Basis Set. *Comp. Mater. Sci*. **1996**, *6*, 15–50.

9 Kresse, G.; Furthmuller, J. Efficient Iterative Schemes for Ab initio Total-Energy Calculations Using a Plane-wave Basis Set. *Phys. Rev. B* **1996**, *54*, 11169–11186.

10 Monkhorst, H. J.; Pack, J. D. Special Points for Brillouin-Zone Integrations. *Phys. Rev. B* **1976**, *13*, 5188–5192.

11 Methfessel, M.; Paxton, A. T. High-Precision Sampling for Brillouin-Zone Integration in Metals. *Phys. Rev. B* **1989**, *40*, 3616–3621.

12 Frisch, M. J. *et al. Gaussian 09, Revision B.01., Vol.*; 2009.

13 Tang, W.; E. Sanville, E.; G. Henkelman, A. Grid-based Bader Analysis Algorithm without Lattice Bias, *J. Phys.: Condens. Matter* **2009**, *21*, 084204.

14 E. Sanville, E.; Kenny, S. D.; Smith, R.; Henkelman, G. An Improved Grid-Based Algorithm for Bader Charge Allocation, *J. Comp. Chem.* **2007**, *28*, 899–908.

15 G. Henkelman, G.; Arnaldsson, A.; Jónsson, H. A. Fast and Robust Algorithm for Bader Decomposition of Charge Density, *Comput. Mater. Sci.* **2006**, *36*, 254–360.

16 Yu, M.; Trinkle, D. R. Accurate and Efficient Algorithm for Bader Charge Integration, *J. Chem. Phys.* **2011**, *134*, 064111.